https://doi.org/10.5194/egusphere-2023-1925
Preprint. Discussion started: 1 September 2023

Intensified future heat extremes linked with increasing ecosystem water limitation

Jasper M.C. Denissen[1,2*], Adriaan J. Teuling[2], Sujan Koirala[1], Markus Reichstein[1], Gianpaolo Balsamo[3], Martha M. Vogel[4], Xin Yu[1] and René Orth[1].

[1]Department for Biogeochemical Integration, Max Planck Institute for Biogeochemistry, Jena, Germany
[2]Hydrology and Quantitative Water Management Group, Wageningen University, Wageningen, The Netherlands
[3]Research Department, European Centre for Medium-Range Weather Forecasts, Reading, United Kingdom
[4]Division of Ecological and Earth Sciences, Natural Sciences Sector, UNESCO, Paris, France

Correspondence to: Jasper M.C. Denissen (jasper.denissen@bgc-jena.mpg.de)

Abstract. Heat extremes have severe implications for human health, ecosystems and the initiation of wildfires. Whereas they are mostly introduced by atmospheric circulation patterns, the intensity of heat extremes is modulated by vegetation functioning associated with soil moisture availability. Thereby, vegetation provides evaporative cooling through transpiration, which can be reduced under water stress. While it has been shown that regional ecosystem water limitation is projected to increase in the future, the respective repercussions on heat extremes remain unclear.

In this study we use projections from eight Earth system models to show that projected changes in heat extremes are amplified by increasing ecosystem water limitation in regions across the globe. We represent ecosystem water limitation with the Ecosystem Limitation Index (ELI) and quantify temperature extremes through the differences between warm-season mean and maximum temperatures. We identify hotspot regions in tropical South America and across Northern Eurasia where relatively strong trends towards increased ecosystem water limitation jointly occur with amplifying heat extremes. This correlation is governed by the magnitude of the ELI trends and the present-day ELI which denotes the land-atmosphere coupling strength determining the temperature sensitivity to evaporative cooling. Many regions where vegetation functions are predominantly energy-limited or transitional in present climate exhibit strong trends towards increasing water limitation and simultaneously experience the largest increases in heat extremes. Therefore, considering the ecosystem's water limitation is key for assessing the intensity of future heat extremes and their corresponding impacts.

1 Introduction

Heat extremes affect ecosystems and society through their implications on human health, crop yields and tree mortality, and the initiation of wildfires (Anderegg et al., 2013; Goulart et al., 2021; McDowell & Allen, 2015; O et al., 2020; Orth et al., 2022; Ruffault et al., 2020; Vogel et al., 2019). In the recent past, temperature extremes have increased in intensity, duration and frequency; these changes are related to climate change (Seneviratne et al., 2021) and they have even accelerated in recent

https://doi.org/10.5194/egusphere-2023-1925
Preprint. Discussion started: 1 September 2023

years in many regions (Seneviratne et al., 2014). In the future, heat extremes are projected to intensify further, alongside the ongoing global warming (Seneviratne et al., 2021).

Hot temperatures can be fueled by dynamic and thermodynamic processes (Harrington et al., 2019; Trenberth et al., 2015). The relevance of atmospheric dynamics for recent heat waves has been highlighted for the case of large-scale blocking patterns which support heat accumulation across consecutive dry days (Cassou et al., 2005; Jézéquel et al., 2018) as well as the entrainment of warm air aloft (Miralles et al., 2014). Also, large-scale circulation patterns advecting warm air, or air from regions with dry soils, have been suggested to contribute to heat waves (Schumacher et al., 2019). Additionally, thermodynamic processes can amplify heat extremes; the land surface determines the partitioning of incoming radiative energy into sensible heating and latent heat (Seneviratne et al., 2010). Changes in this flux partitioning can be induced through soil moisture drying as water-stressed vegetation tends to reduce transpiration; this way, a larger fraction of the incoming energy is available for sensible heating which can lead to elevated temperatures (Budyko, 1974; Denissen et al., 2021; Vogel et al., 2017). As a consequence, circulation-induced rainfall deficits are translated by ecosystem water limitation to reduced evaporative cooling and amplified local temperatures (Miralles et al., 2012; Quesada et al., 2012; Teuling et al., 2010; Ukkola et al., 2018).

It has been shown that climate change may involve regional long-term trends in soil moisture and land-atmosphere coupling (Berg et al., 2017; Berg & Sheffield, 2018; Denissen et al., 2022; Seneviratne et al., 2021; Sippel et al., 2017) and that these can contribute to amplified heat extremes (Lorenz et al., 2016; Seneviratne et al., 2006; Vogel et al., 2017) especially in the case of depletion of soil moisture preceding the warm season (Rasmijn et al., 2018; Stegehuis et al., 2021). In this study, we revisit and complement this previous research with novel indices and by analyzing output from the latest generation of Earth System models from the Coupled Model Intercomparison Project Phase 6 (CMIP6, (Eyring et al., 2016)).In particular we use (i) a recently introduced ecosystem water stress index (Ecosystem Limitation Index (ELI), (Denissen et al., 2020)) which directly captures evaporative cooling and hence links more mechanistically with heat waves than general land-atmosphere coupling indices. Further, the ELI can be used to pinpoint regime transitions, as positive values are indicative of water-limited conditions, while negative values denote ecosystem energy limitation. In addition, for analyzing heat extremes, we (ii) focus on the difference between warm-season average and maximum temperatures, hereafter referred to as temperature excess. While temperature excess is known to be affected by land-atmosphere coupling (Dirmeyer et al., 2021; Donat et al., 2017; Lorenz et al., 2016; Schwingshackl et al., 2018; Seneviratne et al., 2006; Sippel et al., 2017; Ukkola et al., 2018; Vogel et al., 2017), the average temperature is largely driven by large-scale circulation (Cassou et al., 2005; Miralles et al., 2014; Schumacher et al., 2019). This way, we assume that by focusing on the difference between mean and maximum temperatures, we can isolate the thermodynamic component from the dynamic component in heat wave development. This way, we jointly assess trends in ecosystem water limitation and heat extremes in fully coupled CMIP6 simulations from eight state-of-the-art Earth system

https://doi.org/10.5194/egusphere-2023-1925
Preprint. Discussion started: 1 September 2023

models at the monthly time scale and 2˚x2˚ spatial resolution from 1980 – 2100 (Eyring et al., 2016) in order to determine the thermodynamic contribution of the land surface for present and future heat extremes.

2 Materials and Methods

2.1 Ecosystem Limitation Index

The Ecosystem Limitation Index (ELI), formerly referred to as the correlation-difference metric (Denissen et al., 2020), is adapted as follows:

$$ELI = cor(SM',ET') - cor(Ta' \mid SWin',ET')$$

The prime denotes monthly anomalies of soil moisture (SM), terrestrial evaporation (ET), air temperature (Ta) and incoming shortwave radiation (SWin). As ET in some regions is limited more strongly by lack of incoming shortwave radiation (Nemani et al., 2003) and in other regions more strongly by cold temperatures, we test for each grid cell which energy proxy yields the highest correlation with ET (cor(Ta',ET') vs. cor(SWin,ET')), and is hence most relevant in this location, to then use it in the computation of ELI in the respective grid cell (Supplementary Figure 1). Between energy- and water-limited conditions, the ELI expresses different typical sensitivities to energy and water supply: High and positive cor(Ta' | SWin,ET') is indicative of energy-limited conditions, whereas high and positive cor(SM',ET') indicates water-limited conditions. The ELI combines both the relevance of energy and water supply for evaporative cooling by taking the difference between those two correlations, so that positive values denote water-limited conditions and negative values indicate energy-limited conditions. Thereby, the ELI can be used to pin-point transitional areas where regime shifts occur frequently, where ELI is approximately zero. Further, in contrast to other traditional indices such as the Aridity Index that rely on climatological means, the ELI can be used to study (parts of) the seasonal cycle. For a more extensive assessment of air temperature or incoming shortwave radiation and soil moisture as the choices for energy and water proxies as well as a detailed elaboration on the interpretation of ELI, please refer to Denissen et al. (Denissen et al., 2022).

2.2 CMIP6 data

In this study, we use data from the Coupled Model Intercomparison Project (CMIP6, (Eyring et al., 2016)), of which the most important information on the used data is summarized in Table 1. We only selected models that provide i) historical (1980 - 2015) and "worst-case" SSP5-8.5 (2015 - 2100 (O'Neill et al., 2016)) simulations, ii) the necessary variables (Table 1) and iii) sufficient spatial (2˚x2˚ grid cell resolution) and temporal (monthly) resolutions. The maximum daily temperature denotes the maximum daily average temperature per month. By taking the SSP5-8.5 scenario we intend to focus on the climate scenario most influenced by human activity and related emissions of greenhouse gasses.

https://doi.org/10.5194/egusphere-2023-1925
Preprint. Discussion started: 1 September 2023

Table 1. Overview of model details and model output used in this study. The following variables have been downloaded from all the models at the monthly time scale: temperature (tas), root-zone soil moisture (mrso), terrestrial evaporation (hfls), leaf area index (lai), maximum daily temperature (tasmax) and in- and outgoing short- and longwave radiation (rsds,rsus,rlds,rlus). Dynamic vegetation reflects whether or not plant functional traits (PFT) can vary in time, responding to competition for resources. These resources could but do not necessarily include any combination of nitrogen, phosphorus, water and energy. However, the resources considered in this context vary between models. As land use change forcing is identical for all models for the SSP5-8.5 scenario (O'Neill et al., 2016), this column only concerns historical simulations. For historical simulations, land use change forcing comes from the Land Use Harmonization (LUH) 2 v2h product (https://luh.umd.edu/data.shtml) (Hurtt et al., 2011), except if mentioned otherwise. As land cover types might vary between models, land use change forcing effects

https://doi.org/10.5194/egusphere-2023-1925
Preprint. Discussion started: 1 September 2023

might differ as well. *: the first number denotes the version of the historical simulation, whereas the second number indicates
105 the SSP5-8.5 simulation.

https://doi.org/10.5194/egusphere-2023-1925
Preprint. Discussion started: 1 September 2023

Institution	Model	Member	Version*	Dynamic vegetation	Irrigation	Land use change	Citation
Beijing Climate Center (BCC)	BCC-CSM2-MR	r1i1p1f1	v20181126 & v20190314	no	no	yes, explicitly involved in BCC-AVIM2.0	(Wu et al., 2018, 2019; Xin et al., 2019)
Canadian Centre for Climate Modelling and Analysis (CCCma)	CanESM5	r1i1p1f1	v20190429 & v20190429	no	no	yes, for crops.	(Swart, et al., 2019b, 2019a)
Centre National de Recherches Météorologiques (CNRM)	CNRM-ESM2-1	r1i1p1f2	v20181206 & v20191021	no	no	yes	(Seferian, 2018; Séférian et al., 2019; Voldoire, 2019)
Chinese Academy of Sciences (CAS)	FGOALS-g3	r2i1p1f1	v20190828 & v20191216	no	yes	yes	(Li, 2019a, 2019b; Li et al., 2020)
Institute for Numerical Mathematics (INM)	INM-CM4-8	r1i1p1f1	v20190530 & v20190603	no	no	no	(E. Volodin et al., 2019a, 2019b; E. M. Volodin et al., 2018)

https://doi.org/10.5194/egusphere-2023-1925
Preprint. Discussion started: 1 September 2023

Institut Pierre Simon Laplace (IPSL)	IPSL-CM6A-LR	r2i1p1f1	v20180803 & v20191121	no	no	yes	(Boucher et al., 2018, 2019, 2020)
Model for Interdisciplinary Research on Climate (MIROC)	MIROC-ES2L	r1i1p1f2	v20190823 & v20190823	no	no	yes	(Hajima et al., 2019, 2020; Tachiiri et al., 2019)
Met Office Hadley Centre (MOHC)	UKESM1-0-LL	r2i1p1f2	v20190627 & v20190726	yes	no	yes, for crops and pasture.	(Good et al., 2019; Sellar et al., 2019; Tang et al., 2019)

2.3 Pre-processing data

After data acquisition, several steps are taken to assure a meaningful selection of data for the analysis. First, to pin-point the hottest heat extremes, we focus on the three hottest months a year (warm season), defined as the 3 months-of-year with the highest maximum daily temperature averaged decadally. The advantage of considering only the warm season lies in the comparison of concomitant trends of ELI, evaporative fraction (EF) and temperature excess, as these might be subject to seasonal variability. Second, to additionally assure that we are investigating the active vegetation periods during the warm season, which would elicit vegetation responses to anomalies in energy and water supply affecting the surface flux partitioning, all months with Ta < 10˚C and Leaf Area Index (LAI) < 0.5 m2 m-2 are excluded from the analysis. Thereby, we disregard mainly grid cells in sparsely vegetated regions in Central Africa, China and Australia and cold regions in the Northern latitudes (Supplementary Figure 2). This selection of data results in what we refer to in this manuscript as the “warm vegetated land area”. This data is then used to compute the decadal time series of the desired diagnostics, which are ELI, EF and temperature excess. EF is computed as the fraction of the net surface radiation (the sum of all radiative components) that is used to evaporate water. Temperature excess is computed for each grid cell and decade as the difference between the means of (i) the 10 warm-

https://doi.org/10.5194/egusphere-2023-1925
Preprint. Discussion started: 1 September 2023

season average temperatures from the individual years and (ii) the 10 temperature maxima in the individual years. Next to this, we assess ecosystem water limitation with the ELI (Equation 1, (Denissen et al., 2020)).

2.4 Computing Theil-Sen slopes and slope significance

The trends shown in Figure 1 and 4 and Supplementary figures 3, 4 and 6 are based on Theil-Sen slopes (Sen, 1968; Theil, 1992). This approach is insensitive to statistical outliers, as the median slope from a range of slopes through all pairs of points is selected as the best fit. The significance of these slopes is determined based on Kendall's tau statistic from Mann-Kendall tests.

3 Results

https://doi.org/10.5194/egusphere-2023-1925
Preprint. Discussion started: 1 September 2023

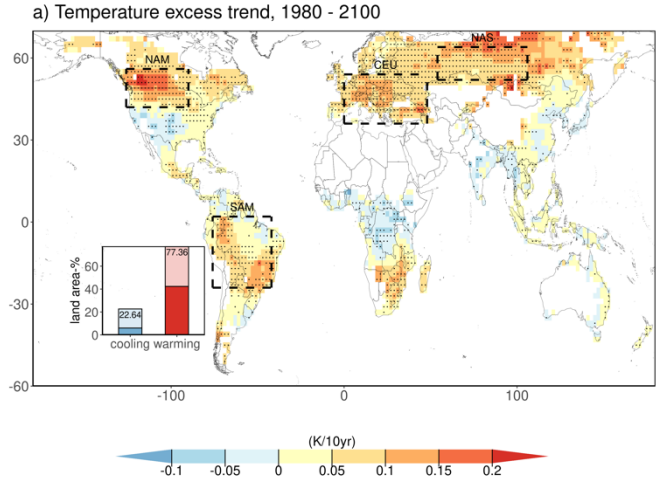

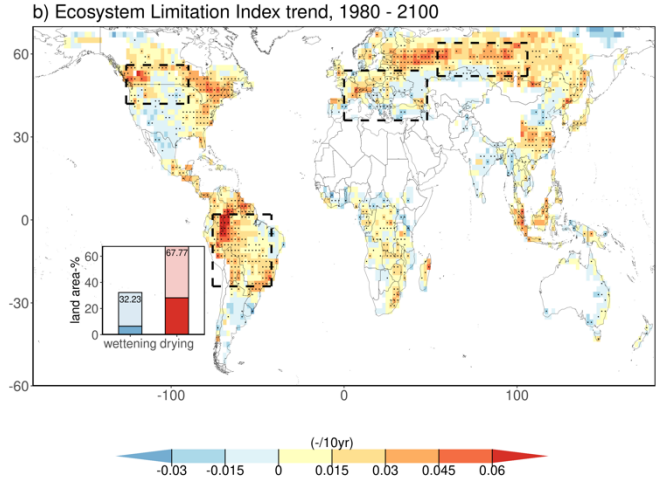

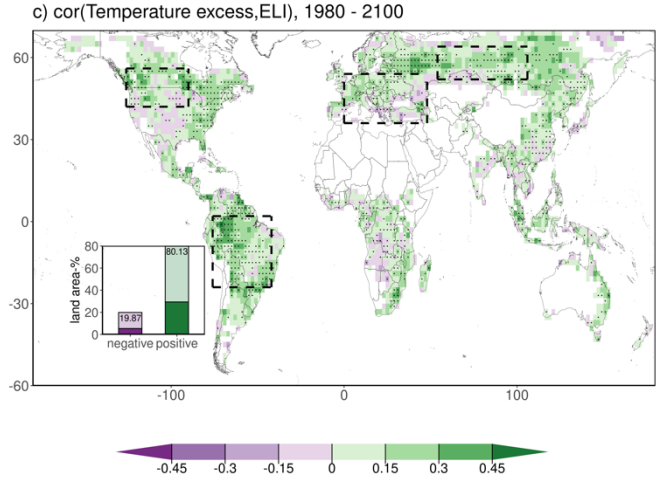

130

https://doi.org/10.5194/egusphere-2023-1925
Preprint. Discussion started: 1 September 2023

Figure 1. Similarity of global patterns of change in temperature excess and ecosystem water limitation. Multi-model means of trends based on decadal time series per respective CMIP6 model of a) temperature excess) and b) Ecosystem Limitation Index (ELI). c) Multi-model means of Kendall's rank correlation coefficient between model-specific time series of ELI and temperature excess. The insets display the fraction of the warm land area that with positive or negative trends or correlations, respectively (at least 6 out of 8 models agreeing on the sign of the trend or correlation are hued darker). Stippling indicates that at least 6 out of 8 CMIP6 models agree on the sign of the trend or correlation. All trends and correlations are calculated over the warm season and are only displayed if at least 5 CMIP6 models have full time series available, such that white areas denote regions with no or insufficient data. The dashed boxes indicate regions of interest, which are regions where temperature excess increases are particularly rapid and spatially coherent: North and South America (NAM and SAM), Central Europe (CEU) and Northern Asia (NAS).

We identify increased temperature excess trends across over 77% of the warm vegetated land area from 1980 - 2100 (Figure 1a). Model confidence is higher for increasing than for decreasing temperature excess (inset plot Figure 1a), as in more than half of the area with increasing temperature excess at least six out of eight CMIP6 models agree, while this is less than a third for decreasing temperature excess (see also Supplementary Figure 3). This reveals high confidence in an accelerated increase of heat extremes compared with warm-season average temperatures.

ELI increases in more than 68% of the warm vegetated land area (Figure 1b), signaling shifts towards water limitation. Generally, models particularly agree on the sign of the ELI increases (stippling in Figure 1b), whereas more uncertainty exists with respect to the magnitude of ELI trends (Supplementary Figure 4). Further, we note that in the mid- to high latitudes, ELI trends are generally temperature controlled, whereas the tropics are more sensitive to incoming shortwave radiation (Supplementary Figure 1), thereby acknowledging and allowing that energy proxies can vary locally.

Spatial patterns of trends in temperature excess and ELI are very similar. Areas with highest temperature excess trends (>0.2 K/10yr) are predominantly characterized by ELI increases (found in 92% of these areas). More importantly, also the temporal evolution of decadal time series of temperature excess and ELI is similar in many regions. This is evidenced by significant correlations in many areas (Figure 1c, Supplementary Figure 5), suggesting that increasing ELI contributes to hotter temperature extremes. We also find regions with insignificant and even negative correlations such as the Sahel, Kazakhstan and parts of North America. As plant transpiration scales with LAI, this limits the ability of the scarce vegetation present in such regions to provide sufficient evaporative cooling, possibly rendering correlations insignificant. Further deviations from a positive relationship between temperature excess and ELI might result from alternative processes such as (changes in) advection of warm air masses through large-scale circulation patterns.

https://doi.org/10.5194/egusphere-2023-1925
Preprint. Discussion started: 1 September 2023

Furthermore, in order to illustrate the physical link between ELI and temperature excess, which presumably is through evaporative cooling, we analyze terrestrial evaporation normalized by net surface radiation. The resulting EF links the surface energy and water balances. The EF is generally decreasing in the four regions of interest with high agreement between individual models (Supplementary Figure 6a). Moreover, EF is generally significantly correlated with both temperature excess and ELI, respectively, establishing the physical link between these quantities. This way, in more than 89% of the warm vegetated land area, trends in EF fraction are negatively correlated with temperature excess, meaning that a decreasing (increasing) trend in EF, renders more (less) energy available for sensible heating, which elevates (reduces) heat extremes (Supplementary Figure 6b). In about 80% of the warm vegetated land area, the correlation between EF and ELI is negative (Supplementary Figure 6c), verifying that a shift towards ecosystem water limitation jointly occurs with the expected decreases in evaporative cooling. Some regions, such as central US, the Mediterranean and Northern Mongolia, exhibit insignificant or even positive correlations, possibly pointing to other processes such as irrigation and/or land use changes (Table 1).

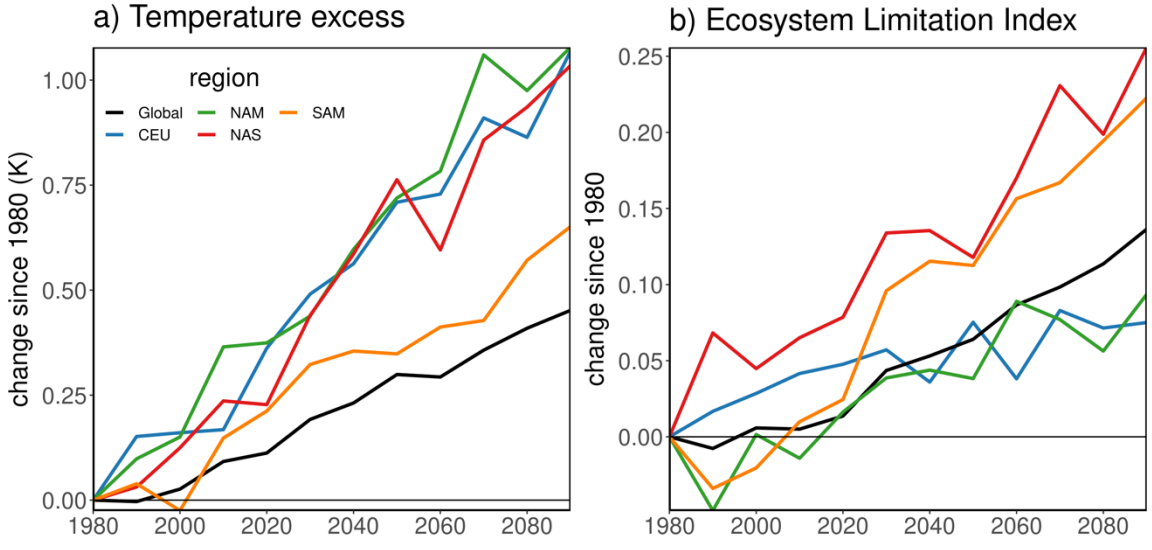

Figure 2. Changes in global and regional temperature excess with increasing ecosystem water limitation. Temporal evolution of a) temperature excess and of b) Ecosystem Limitation Index (ELI) globally and for the regions of interest. Solid lines depict multi-model mean time series. Global and regional averages are calculated over land grid cells that have complete time series for all models and variables and are weighted according to the surface area per grid cell.

Next, we compare the temporal evolution of temperature excess and ELI averaged across the regions of interest and the entire warm vegetated land area between historical and future time periods. Figure 2a shows a steady global increase of temperature excess, with warm-season maximum temperature experiencing an additional 0.5K warming with respect to the average warm-season temperature over 1980 – 2100. In all regions of interest but SAM, temperature excess is increasing over twice as fast

https://doi.org/10.5194/egusphere-2023-1925
Preprint. Discussion started: 1 September 2023

as the global average. Even though uncertainty in temperature excess exists between individual models (Supplementary Figure 7a), the majority of models agree both globally and regionally that temperature excess is significantly increasing.

ELI trends differ more strongly in magnitude across the regions of interest than the temperature excess trends (Figure 2b). While underlying ELI trends from individual models generally tend to display positive ELI trends, there is a larger spread both in magnitude and in sign (Supplementary Figure 7b). This indicates different contributions of the ELI to the temperature excess trends between models (Supplementary Figure 5) and regions; while the ELI contribution is particularly strong in NAS and SAM, as can also be seen from the correlations in Figure 1c, it is weaker but still considerable in CEU and NAM where probably other processes play a role such as changes in large-scale circulation patterns or boundary layer dynamics. Further, most significant trends in Supplementary Figure 7b are positive, underlining a higher confidence of the model ensemble to project increasing rather than decreasing ecosystem water limitation.

During 1980 – 2020, temperature excess computed from ERA5-Land data lies largely within the envelope of the individual CMIP6 models (Supplementary Figure 8a, "ERA5-Land analysis" in Supplementary material). As such, the temperature excess findings from individual CMIP6 models are not implausible. As the ERA5-Land dataset is supported by the comprehensive assimilation of available observations, the similarity of the CMIP6 model results in terms of temperature excess demonstrates a successful validation of the models considered here. This is further corroborated by surface air temperature extremes from CMIP5 and CMIP6, that compare well with observation-based data sets, albeit with model-specific performance that varies in space and time (Thorarinsdottir et al., 2020). At the same time, the CMIP6-based ELI is only partly corroborated by the ERA5-Land reanalysis data from 1980 – 2020 (Supplementary Figure 8b), as globally and in half the regions of interest the reanalysis-based ELI exceeds the CMIP6 envelope. Note that the ERA5-Land reanalysis is not supported as much by assimilated observations in the case of ELI compared to temperature excess, as ELI is based on ET and (root-zone) soil moisture which are not readily observed across the globe. This way, ERA5-Land estimates of the global ELI evolution are subject to uncertainty, and while it provides an independent reference for comparing the CMIP6 model results it is itself based on the land surface model dynamics underlying the ERA5-Land dataset. Next to that, differences could arise due to different land cover maps underlying respective simulations from ERA5-Land and the CMIP6 models.

The tendency of temperature excess to be elevated in response to increasing ecosystem water limitation becomes even clearer when only grid cells where at least six out of eight CMIP6 models agree on the sign of the temperature excess trends are included. This is evidenced by a stronger increase of ELI in regions with robust temperature excess trends (Supplementary Figure 9). ELI trends are even larger for regions with robust and positive temperature excess trends. At the same time no clear trends in ELI are found for regions with robust and negative temperature excess trends. This suggests that factors other than evaporative cooling, such as changes in circulation, render the temperature excess trends negative in these regions.

https://doi.org/10.5194/egusphere-2023-1925
Preprint. Discussion started: 1 September 2023

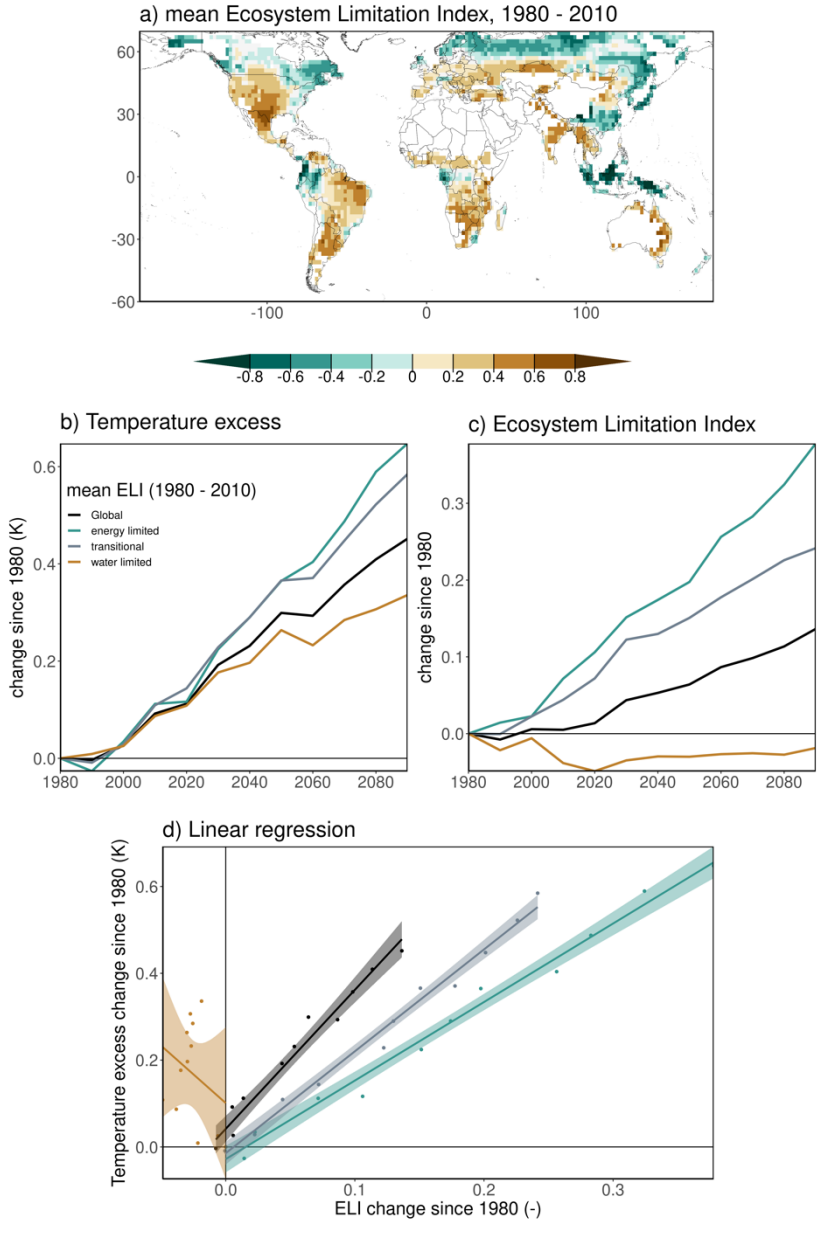

Figure 3. Relation between temperature excess and ecosystem water limitation. a) Multi-model mean Ecosystem Limitation Index (1980 - 2010). Solid lines depict the time series of multi-model means inferred from globally (black) and regionally (colored) decadally averaged model simulations for b) temperature excess and c) Ecosystem Limitation Index. The classification is defined based on the model-specific mean ELI over 1980 - 2010 (Supplementary Figure 10): Energy limited (ELI < -0.2), transitional (-0.2 < ELI < 0.2) and water limited (ELI > 0.2). d) Points denote the global (black) and regional (colored) decadal multi-model means of ELI (x-axis) and temperature excess (y-axis), expressed as change since 1980. The lines denote linear regressions, with a shaded colored 95% confidence interval. Land grid cells that do not have complete time

https://doi.org/10.5194/egusphere-2023-1925
Preprint. Discussion started: 1 September 2023

series for all models are excluded (white regions, Methods). Global and regional averages are weighted according to the surface area per grid cell.

The sensitivity of temperature excess to ELI trends is expected to depend on the initial regime: In initially energy-limited grid cells, ecosystems can provide ample evaporative cooling. Hence, in such grid cells shifts towards water limitation, evidenced by positive ELI trends, should not amount to large changes in surface flux partitioning, nor in temperature excess. We expect the opposite in initially transitional grid cells, where evaporative cooling should be sensitive to ELI trends. In water-limited grid cells, vegetation activity might be too low to provide ample evaporative cooling, such that shifts towards ecosystem water limitation cannot decrease evaporative cooling further. To test this hypothesis, we classify all grid cells based on their respective mean ELI over 1980 - 2010 (Figure 3a) to define energy-limited (ELI < -0.2), transitional (-0.2 < ELI < 0.2) and water-limited (ELI > 0.2) conditions. We analyze temperature excess trends across these three regimes and find that over initially water-limited areas they are below the global average, while trends over initially transitional or energy-limited areas are above the global average (Figure 3b). This is against our initial expectation but can be explained by the corresponding ELI trends which are much more pronounced in energy-limited regions (Figure 3c), leading to more often occurring water-limited conditions in these areas. However, in initially water-limited regions, temperature excess increases despite ELI remaining fairly constant over the study period, pointing to other processes affecting temperature excess. Moving beyond trends we also analyze the sensitivity of decadal temperature excess with respect to ELI for energy-limited vs. transitional vs. water-limited areas and find the strongest relationship in the case of transitional areas (Figure 3d), as evidenced by the largest increase in temperature excess with ELI. This confirms that changes in transitional areas temperature excess trends are most sensitive to ELI trends.

To quantify the strength of the relationships displayed in Figure 3d we compute correlations for the relationships shown for the three regimes, respectively (Supplementary Figure 11a). This suggests again the stronger link between ELI and temperature excess, especially in transitional, but also energy-limited areas resulting from the strong ELI trends moving these areas towards water-limitation. To study the relevance of spatial variability across the grid cells that are initially energy- or water-limited or transitional for the correlation estimates, the grid-specific time series of temperature excess and ELI are bootstrapped and displayed as boxplots in Supplementary Figure 10a, with overall similar results. Substantial variability exists across model-specific correlations (Supplementary Figure 11b,c). Although the models generally agree on the signs of the correlations, the magnitudes of correlations differ strongly, possibly relating to different representations of land-atmosphere coupling and resulting differences in initial ELI states and trends (Supplementary Figure 5 and 10).

https://doi.org/10.5194/egusphere-2023-1925
Preprint. Discussion started: 1 September 2023

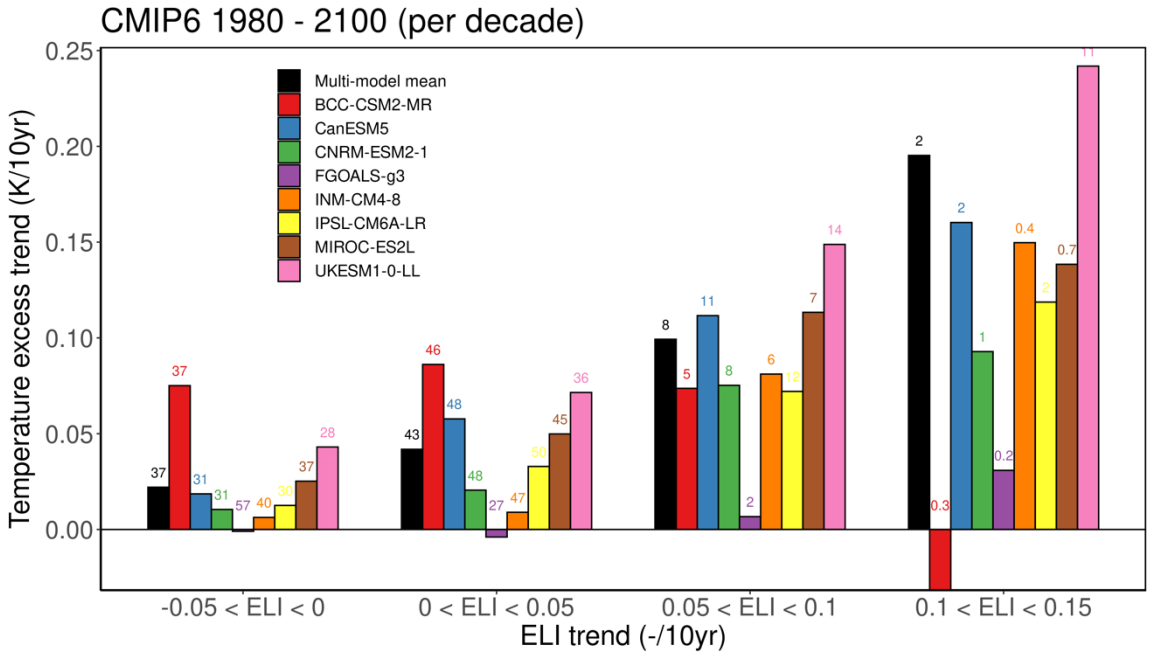

Figure 4. Temperature excess trends increase with stronger trends in ecosystem water limitation. The bars denote the multi-model mean and model-specific temperature excess trends (y-axis) binned according to their respective ELI trends (x-axis) for the multi-model mean trends (black) and all individual models (colors). The numbers display the fraction of warm vegetated land area in which respective temperature excess and ELI trends occur and do not add up to 100%, because there are values outside of the defined bins on the x-axis.

In order to further analyze the role of the magnitude of ELI trends for the coinciding temperature excess trends, we group the global grid cells with respect to their ELI trends and show the multi-model mean and model-specific temperature excess trends (Figure 4). Higher temperature excess trends correspond with stronger increasing ELI trends. Such strong increases in ELI indicate more often occurring water-limited conditions, potentially also during heat wave events, such that temperature excess gets more sensitive to ELI. Analyzing results from individual models shows that stronger ELI trends are associated with stronger trends in temperature excess in almost all models, albeit with substantial variability between individual models, owing to different representations and strength of land-atmosphere coupling.

4 Discussion

Our findings corroborate earlier research which demonstrated the relevance of soil moisture to (future) heat extremes via its control on surface flux partitioning based on idealized Earth system model experiments in which long-term soil moisture trends are artificially removed (Fischer et al., 2007; Lorenz et al., 2016; Schwingshackl et al., 2018; Seneviratne et al., 2006; Vogel et al., 2017, 2018). While our correlative analysis cannot establish the causal link nor disentangle the direction of causality

https://doi.org/10.5194/egusphere-2023-1925
Preprint. Discussion started: 1 September 2023

between land surface dynamics and heat extremes to the same extent, it benefits from fully coupled simulations without artificial tweaking the water balances, such that it effectively complements the existing body of research. We note that temperature excess is not exclusively driven by land-atmosphere coupling, and the findings presented here merely stress the importance of considering ELI in this context.

While the correlation between ELI and heat wave temperatures is robust across models, we find substantial differences between individual models in terms of the strength of this link (e.g. Figure 4 and Supplementary Figures 5, 6, 7 and 11). This could be related to a different representation of land-atmosphere interactions in general, which could be due to e.g. different soil moisture layers and depths, as well as different underlying soil and vegetation types. Additionally, models might use different vegetation water stress functions, some of which are poorly constrained by theory (De Kauwe et al., 2017; Martínez-de la Torre et al., 2019; Ukkola, Kauwe, et al., 2016). Further, not all models include dynamic vegetation, irrigation and land use change (Table 1). Another reason might be that measurements of soil moisture and terrestrial evaporation are scarce, such that large-scale observational constraints for these key quantities have been lacking and are only recently available following the advent of machine-learning techniques to efficiently interpolate global gridded datasets from the available in-situ measurements (Jung et al., 2019; O & Orth, 2021). Additionally, the vegetation's response to soil moisture drying is difficult to capture due to heterogeneous soil and vegetation characteristics and limited observational constraints for rooting depths and soil moisture dynamics in respective soil layers. Next to those processes, the effects of ELI on temperature excess can be obscured by land use and circulation change. Although disentangling such effects would be insightful, we consider a comprehensible analysis out of scope for this study. However, despite apparent differences in processes represented in the models, we still find mostly significant positive correlations between temperature excess and ELI in most models (Supplementary Figure 5).

Further, despite the apparent difficulty that Earth System Models experience with representing soil moisture trends and related trends in land-atmosphere processes (Albergel et al., 2013; Berg et al., 2017; Berg & Sheffield, 2018; Greve et al., 2019), widespread shifts towards water limitation are robustly projected (Figure 1; (Denissen et al., 2022; Teuling, 2018; Ukkola et al., 2018)). Further highlighting the complex nature of land-atmosphere interactions, we note that ecosystem water limitation is not only affected by climate, but also by changes in vegetation physiology (e.g. stomatal regulation) and structure (e.g. LAI) in response to increasing CO2 (CO2 fertilization; (Donohue et al., 2013; Ukkola, Prentice, et al., 2016; Walker et al., 2021; Zhu et al., 2016)), which has also been shown to modulate heat extremes (Lemordant & Gentine, 2019). This way, changes of both CO2 and climate jointly affect ELI which in turn influences heat wave magnitudes. Given this situation, future research should focus on the link between ELI and heat wave intensities using observation-based datasets, particularly as longer-term interpolations or reconstructions of key variables become available. This can help to corroborate model-based findings, and to constrain the variable relevance of ELI across models.

https://doi.org/10.5194/egusphere-2023-1925
Preprint. Discussion started: 1 September 2023

Finally, we focus on the intensity of the heat extremes by considering temperature only rather than more impact-relevant indices. Heat stress for humans is dependent not only on temperature, but also on wind speed and humidity (Buzan & Huber, 2020; Matthews, 2018). Through reduced evaporative cooling and increased entrainment of dry air above the atmospheric boundary layer, the lethality of heat extremes above dry soils can be reduced (Wouters et al., 2022). In this study, we find an increasing temperature excess alongside increasing EF in 18% of the warm vegetated land area (Supplementary Figure 6b), which suggests potentially higher heat stress than reflected by temperature alone as terrestrial evaporation can increase humidity and related lethality. On the other hand, combined hot and dry conditions can lead to increased wildfires (O et al., 2020) and can be associated with severe impacts on agriculture and infrastructure. In that perspective, our results on the correspondence between increased ecosystem water limitation and amplified heat waves confirm findings from Teuling et al. (Teuling, 2018) indicating that droughts in Europe will become hotter under future warming. This is in line with future projections, suggesting that concurrent hot and dry extremes will continue to increase in future (Seneviratne et al., 2021; Vogel et al., 2020).

5 Conclusion

In conclusion, we show the ability of the land surface to modulate the intensity of future heat extremes. In this context we focus on novel indices by focusing on ecosystem water limitation and the temperature excess between warm-season mean and maximum temperatures. This way, we find a widespread increase in temperature excess in ~77% of our study area. We identify several regions of interest where temperature excess is increasing more rapidly than the global mean. In large parts of these regions, these increases jointly occur with trends towards ecosystem water limitation which lead to reduced evaporative cooling. Thereby, the relevance of trends in ecosystem water limitation for trends in temperature excess depends on (i) the magnitude of the ELI trends, which is largest in initially energy-limited and transitional areas, and (ii) the initial ELI regime as (maximum) temperatures are more sensitive to evaporative cooling in a transitional regime.

Finally, identifying regions where ELI trends and related evaporative cooling are important for future heat extremes can inform long-term adaptation strategies. Human activities play a key role here, as we can implement agricultural practices and/or tillage, irrigation and land cover management, afforestation and city greening to mitigate the impact of heat extremes (Schwaab et al., 2021; Sillmann et al., 2017).

Data and code availability

The CMIP6 model simulation data is freely available from Google cloud CMIP6 public data: https://pangeo-data.github.io/pangeo-cmip6-cloud/. All the data used in this analysis will be made publicly available in a data repository which can be assessed vai Zenodo.

The scripts to acquire and aggregate CMIP6 data are publicly available (https://doi.org/10.5281/zenodo.5900393, (Koirala, 2022)). All the code written and used in this analysis will be made available from a code repository on Zenodo.

https://doi.org/10.5194/egusphere-2023-1925
Preprint. Discussion started: 1 September 2023

Author contributions

R.O., A.J.T. and J.M.C.D. jointly designed the study. J.M.C.D. performed the analyses. All authors contributed to the writing of the paper, the discussion and interpretation of the results.

Competing Interest Statement

The authors declare no competing interests.

Acknowledgements

R.O. is supported through funding from the German Research Foundation (Emmy Noether Grant 391059971). We thank the respective climate modelling groups for making their model output available within the Coupled Model Intercomparison Project Phase 6 (CMIP6) ensemble. Further, I want to acknowledge the fruitful discussions within the Hydrosphere-Biosphere-Climate Interactions group in the Biogeochemical Integration Department of the Max Planck Institute for Biogeochemistry that have contributed to the interpretation of the results and design of the figures. A special thanks to Sujan Koirala for making the scripts to download CMIP6 data from Google cloud CMIP6 public data publicly available and supporting whenever issues came up. Another special thanks to Ulrich Weber for downloading and aggregating the reanalysis data used in this study.

References

Albergel, C., Dorigo, W., Reichle, R. H., Balsamo, G., Rosnay, P. de, Muñoz-Sabater, J., Isaksen, L., Jeu, R. de, & Wagner, W. (2013). Skill and Global Trend Analysis of Soil Moisture from Reanalyses and Microwave Remote Sensing. *Journal of Hydrometeorology*, *14*(4), 1259–1277. https://doi.org/10.1175/JHM-D-12-0161.1

Anderegg, W. R. L., Kane, J. M., & Anderegg, L. D. L. (2013). Consequences of widespread tree mortality triggered by drought and temperature stress. *Nature Climate Change*, *3*(1), Article 1. https://doi.org/10.1038/nclimate1635

Berg, A., & Sheffield, J. (2018). Climate Change and Drought: The Soil Moisture Perspective. *Current Climate Change Reports*, *4*(2), 180–191. https://doi.org/10.1007/s40641-018-0095-0

Berg, A., Sheffield, J., & Milly, P. C. D. (2017). Divergent surface and total soil moisture projections under global warming. *Geophysical Research Letters*, *44*(1), 236–244. https://doi.org/10.1002/2016GL071921

Boucher, O., Denvil, S., Levavasseur, G., Cozic, A., Caubel, A., Foujols, M.-A., Meurdesoif, Y., Cadule, P., Devilliers, M., Dupont, E., & Lurton, T. (2019). *IPSL IPSL-CM6A-LR model output prepared for CMIP6 ScenarioMIP* [Data set]. Earth System Grid Federation. https://doi.org/10.22033/ESGF/CMIP6.1532

https://doi.org/10.5194/egusphere-2023-1925
Preprint. Discussion started: 1 September 2023

Boucher, O., Denvil, S., Levavasseur, G., Cozic, A., Caubel, A., Foujols, M.-A., Meurdesoif, Y., Cadule, P., Devilliers, M., Ghattas, J., Lebas, N., Lurton, T., Mellul, L., Musat, I., Mignot, J., & Cheruy, F. (2018). *IPSL IPSL-CM6A-LR model output prepared for CMIP6 CMIP historical* [Data set]. Earth System Grid Federation. https://doi.org/10.22033/ESGF/CMIP6.5195

Boucher, O., Servonnat, J., Albright, A. L., Aumont, O., Balkanski, Y., Bastrikov, V., Bekki, S., Bonnet, R., Bony, S., Bopp, L., Braconnot, P., Brockmann, P., Cadule, P., Caubel, A., Cheruy, F., Codron, F., Cozic, A., Cugnet, D., D'Andrea, F., … Vuichard, N. (2020). Presentation and Evaluation of the IPSL-CM6A-LR Climate Model. *Journal of Advances in Modeling Earth Systems*, *12*(7), e2019MS002010. https://doi.org/10.1029/2019MS002010

Budyko, M. I. (1974). *Climate and life*. Academic Press. https://scholar.google.com/scholar_lookup?title=Climate+and+life&author=Budyko%2C+M.+I.+%28Mikhail+Ivanovich%29&publication_year=1974

Buzan, J. R., & Huber, M. (2020). Moist Heat Stress on a Hotter Earth. *Annual Review of Earth and Planetary Sciences*, *48*(1), 623–655. https://doi.org/10.1146/annurev-earth-053018-060100

Cassou, C., Terray, L., & Phillips, A. S. (2005). Tropical Atlantic Influence on European Heat Waves. *Journal of Climate*, *18*(15), 2805–2811. https://doi.org/10.1175/JCLI3506.1

De Kauwe, M. G., Medlyn, B. E., Walker, A. P., Zaehle, S., Asao, S., Guenet, B., Harper, A. B., Hickler, T., Jain, A. K., Luo, Y., Lu, X., Luus, K., Parton, W. J., Shu, S., Wang, Y.-P., Werner, C., Xia, J., Pendall, E., Morgan, J. A., … Norby, R. J. (2017). Challenging terrestrial biosphere models with data from the long-term multifactor Prairie Heating and CO2 Enrichment experiment. *Global Change Biology*, *23*(9), 3623–3645. https://doi.org/10.1111/gcb.13643

Denissen, J. M. C., Orth, R., Wouters, H., Miralles, D. G., van Heerwaarden, C. C., Vilà-Guerau de Arellano, J., & Teuling, A. J. (2021). Soil moisture signature in global weather balloon soundings. *Npj Climate and Atmospheric Science*, *4*(1), Article 1. https://doi.org/10.1038/s41612-021-00167-w

Denissen, J. M. C., Teuling, A. J., Pitman, A. J., Koirala, S., Migliavacca, M., Li, W., Reichstein, M., Winkler, A. J., Zhan, C., & Orth, R. (2022). Widespread shift from ecosystem energy to water limitation with climate change. *Nature Climate Change*, *12*(7), Article 7. https://doi.org/10.1038/s41558-022-01403-8

Denissen, J. M. C., Teuling, A. J., Reichstein, M., & Orth, R. (2020). Critical Soil Moisture Derived From Satellite Observations Over Europe. *Journal of Geophysical Research: Atmospheres*, *125*(6), e2019JD031672. https://doi.org/10.1029/2019JD031672

https://doi.org/10.5194/egusphere-2023-1925
Preprint. Discussion started: 1 September 2023

Dirmeyer, P. A., Balsamo, G., Blyth, E. M., Morrison, R., & Cooper, H. M. (2021). Land-Atmosphere Interactions Exacerbated the Drought and Heatwave Over Northern Europe During Summer 2018. *AGU Advances*, *2*(2), e2020AV000283. https://doi.org/10.1029/2020AV000283

Donat, M. G., Pitman, A. J., & Seneviratne, S. I. (2017). Regional warming of hot extremes accelerated by surface energy fluxes. *Geophysical Research Letters*, *44*(13), 7011–7019. https://doi.org/10.1002/2017GL073733

Donohue, R. J., Roderick, M. L., McVicar, T. R., & Farquhar, G. D. (2013). Impact of CO2 fertilization on maximum foliage cover across the globe's warm, arid environments. *Geophysical Research Letters*, *40*(12), 3031–3035. https://doi.org/10.1002/grl.50563

Eyring, V., Bony, S., Meehl, G. A., Senior, C. A., Stevens, B., Stouffer, R. J., & Taylor, K. E. (2016). Overview of the Coupled Model Intercomparison Project Phase 6 (CMIP6) experimental design and organization. *Geoscientific Model Development*, *9*(5), 1937–1958. https://doi.org/10.5194/gmd-9-1937-2016

Fischer, E. M., Seneviratne, S. I., Lüthi, D., & Schär, C. (2007). Contribution of land-atmosphere coupling to recent European summer heat waves. *Geophysical Research Letters*, *34*(6). https://doi.org/10.1029/2006GL029068

Good, P., Sellar, A., Tang, Y., Rumbold, S., Ellis, R., Kelley, D., Kuhlbrodt, T., & Walton, J. (2019). *MOHC UKESM1.0-LL model output prepared for CMIP6 ScenarioMIP* [Data set]. Earth System Grid Federation. https://doi.org/10.22033/ESGF/CMIP6.1567

Goulart, H. M. D., van der Wiel, K., Folberth, C., Balkovic, J., & van den Hurk, B. (2021). Storylines of weather-induced crop failure events under climate change. *Earth System Dynamics*, *12*(4), 1503–1527. https://doi.org/10.5194/esd-12-1503-2021

Greve, P., Roderick, M. L., Ukkola, A. M., & Wada, Y. (2019). The aridity Index under global warming. *Environmental Research Letters*, *14*(12), 124006. https://doi.org/10.1088/1748-9326/ab5046

Hajima, T., Abe, M., Arakawa, O., Suzuki, T., Komuro, Y., Ogura, T., Ogochi, K., Watanabe, M., Yamamoto, A., Tatebe, H., Noguchi, M. A., Ohgaito, R., Ito, A., Yamazaki, D., Ito, A., Takata, K., Watanabe, S., Kawamiya, M., & Tachiiri, K. (2019). *MIROC MIROC-ES2L model output prepared for CMIP6 CMIP historical* [Data set]. Earth System Grid Federation. https://doi.org/10.22033/ESGF/CMIP6.5602

Hajima, T., Watanabe, M., Yamamoto, A., Tatebe, H., Noguchi, M. A., Abe, M., Ohgaito, R., Ito, A., Yamazaki, D., Okajima, H., Ito, A., Takata, K., Ogochi, K., Watanabe, S., & Kawamiya, M. (2020). Development of the MIROC-ES2L Earth system model and the evaluation of biogeochemical processes and feedbacks. *Geoscientific Model Development*, *13*(5), 2197–2244. https://doi.org/10.5194/gmd-13-2197-2020

https://doi.org/10.5194/egusphere-2023-1925
Preprint. Discussion started: 1 September 2023

Harrington, L. J., Otto, F. E. L., Cowan, T., & Hegerl, G. C. (2019). Circulation analogues and uncertainty in the time-evolution of extreme event probabilities: Evidence from the 1947 Central European heatwave. *Climate Dynamics*, *53*(3), 2229–2247. https://doi.org/10.1007/s00382-019-04820-2

Hurtt, G. C., Chini, L. P., Frolking, S., Betts, R. A., Feddema, J., Fischer, G., Fisk, J. P., Hibbard, K., Houghton, R. A., Janetos, A., Jones, C. D., Kindermann, G., Kinoshita, T., Klein Goldewijk, K., Riahi, K., Shevliakova, E., Smith, S., Stehfest, E., Thomson, A., … Wang, Y. P. (2011). Harmonization of land-use scenarios for the period 1500–2100: 600 years of global gridded annual land-use transitions, wood harvest, and resulting secondary lands. *Climatic Change*, *109*(1), 117. https://doi.org/10.1007/s10584-011-0153-2

Jézéquel, A., Cattiaux, J., Naveau, P., Radanovics, S., Ribes, A., Vautard, R., Vrac, M., & Yiou, P. (2018). Trends of atmospheric circulation during singular hot days in Europe. *Environmental Research Letters*, *13*(5), 054007. https://doi.org/10.1088/1748-9326/aab5da

Jung, M., Koirala, S., Weber, U., Ichii, K., Gans, F., Camps-Valls, G., Papale, D., Schwalm, C., Tramontana, G., & Reichstein, M. (2019). The FLUXCOM ensemble of global land-atmosphere energy fluxes. *Scientific Data*, *6*(1), Article 1. https://doi.org/10.1038/s41597-019-0076-8

Koirala, S. (2022). *Python script to download CMIP6 data from Pangeo Gallery*. https://doi.org/10.5281/zenodo.5900393

Lemordant, L., & Gentine, P. (2019). Vegetation Response to Rising CO2 Impacts Extreme Temperatures. *Geophysical Research Letters*, *46*(3), 1383–1392. https://doi.org/10.1029/2018GL080238

Li, L. (2019a). *CAS FGOALS-g3 model output prepared for CMIP6 CMIP historical* [Data set]. Earth System Grid Federation. https://doi.org/10.22033/ESGF/CMIP6.3356

Li, L. (2019b). *IPCC DDC: CAS FGOALS-g3 model output prepared for CMIP6 ScenarioMIP* [Data set]. World Data Center for Climate (WDCC) at DKRZ. https://www.wdc-climate.de/ui/entry?acronym=C6SPCASFGO

Li, L., Yu, Y., Tang, Y., Lin, P., Xie, J., Song, M., Dong, L., Zhou, T., Liu, L., Wang, L., Pu, Y., Chen, X., Chen, L., Xie, Z., Liu, H., Zhang, L., Huang, X., Feng, T., Zheng, W., … Wei, J. (2020). The Flexible Global Ocean-Atmosphere-Land System Model Grid-Point Version 3 (FGOALS-g3): Description and Evaluation. *Journal of Advances in Modeling Earth Systems*, *12*(9), e2019MS002012. https://doi.org/10.1029/2019MS002012

Lorenz, R., Argüeso, D., Donat, M. G., Pitman, A. J., van den Hurk, B., Berg, A., Lawrence, D. M., Chéruy, F., Ducharne, A., Hagemann, S., Meier, A., Milly, P. C. D., & Seneviratne, S. I. (2016). Influence of land-atmosphere feedbacks on temperature and precipitation extremes in the GLACE-CMIP5 ensemble. *Journal of Geophysical Research: Atmospheres*, *121*(2), 607–623. https://doi.org/10.1002/2015JD024053

https://doi.org/10.5194/egusphere-2023-1925
Preprint. Discussion started: 1 September 2023

Martínez-de la Torre, A., Blyth, E. M., & Robinson, E. L. (2019). Evaluation of Drydown Processes in Global Land Surface and Hydrological Models Using Flux Tower Evapotranspiration. *Water*, *11*(2), Article 2. https://doi.org/10.3390/w11020356

Matthews, T. (2018). Humid heat and climate change. *Progress in Physical Geography: Earth and Environment*, *42*(3), 391–405. https://doi.org/10.1177/0309133318776490

McDowell, N. G., & Allen, C. D. (2015). Darcy's law predicts widespread forest mortality under climate warming. *Nature Climate Change*, *5*(7), Article 7. https://doi.org/10.1038/nclimate2641

Miralles, D. G., Teuling, A. J., van Heerwaarden, C. C., & Vilà-Guerau de Arellano, J. (2014). Mega-heatwave temperatures due to combined soil desiccation and atmospheric heat accumulation. *Nature Geoscience*, *7*(5), Article 5. https://doi.org/10.1038/ngeo2141

Miralles, D. G., van den Berg, M. J., Teuling, A. J., & de Jeu, R. a. M. (2012). Soil moisture-temperature coupling: A multiscale observational analysis. *Geophysical Research Letters*, *39*(21). https://doi.org/10.1029/2012GL053703

Nemani, R. R., Keeling, C. D., Hashimoto, H., Jolly, W. M., Piper, S. C., Tucker, C. J., Myneni, R. B., & Running, S. W. (2003). Climate-Driven Increases in Global Terrestrial Net Primary Production from 1982 to 1999. *Science*, *300*(5625), 1560–1563. https://doi.org/10.1126/science.1082750

O, S., Hou, X., & Orth, R. (2020). Observational evidence of wildfire-promoting soil moisture anomalies. *Scientific Reports*, *10*(1), Article 1. https://doi.org/10.1038/s41598-020-67530-4

O, S., & Orth, R. (2021). Global soil moisture data derived through machine learning trained with in-situ measurements. *Scientific Data*, *8*(1), Article 1. https://doi.org/10.1038/s41597-021-00964-1

O'Neill, B. C., Tebaldi, C., van Vuuren, D. P., Eyring, V., Friedlingstein, P., Hurtt, G., Knutti, R., Kriegler, E., Lamarque, J.-F., Lowe, J., Meehl, G. A., Moss, R., Riahi, K., & Sanderson, B. M. (2016). The Scenario Model Intercomparison Project (ScenarioMIP) for CMIP6. *Geoscientific Model Development*, *9*(9), 3461–3482. https://doi.org/10.5194/gmd-9-3461-2016

Orth, R., O, S., Zscheischler, J., Mahecha, M. D., & Reichstein, M. (2022). Contrasting biophysical and societal impacts of hydro-meteorological extremes. *Environmental Research Letters*, *17*(1), 014044. https://doi.org/10.1088/1748-9326/ac4139

Quesada, B., Vautard, R., Yiou, P., Hirschi, M., & Seneviratne, S. I. (2012). Asymmetric European summer heat predictability from wet and dry southern winters and springs. *Nature Climate Change*, *2*(10), Article 10. https://doi.org/10.1038/nclimate1536

Rasmijn, L. M., van der Schrier, G., Bintanja, R., Barkmeijer, J., Sterl, A., & Hazeleger, W. (2018). Future equivalent of 2010 Russian heatwave intensified by weakening soil moisture constraints. *Nature Climate Change*, *8*(5), Article 5. https://doi.org/10.1038/s41558-018-0114-0

https://doi.org/10.5194/egusphere-2023-1925
Preprint. Discussion started: 1 September 2023

Ruffault, J., Curt, T., Moron, V., Trigo, R. M., Mouillot, F., Koutsias, N., Pimont, F., Martin-StPaul, N., Barbero, R., Dupuy, J.-L., Russo, A., & Belhadj-Khedher, C. (2020). Increased likelihood of heat-induced large wildfires in the Mediterranean Basin. *Scientific Reports*, *10*(1), Article 1. https://doi.org/10.1038/s41598-020-70069-z

Schumacher, D. L., Keune, J., van Heerwaarden, C. C., Vilà-Guerau de Arellano, J., Teuling, A. J., & Miralles, D. G. (2019). Amplification of mega-heatwaves through heat torrents fuelled by upwind drought. *Nature Geoscience*, *12*(9), Article 9. https://doi.org/10.1038/s41561-019-0431-6

Schwaab, J., Meier, R., Mussetti, G., Seneviratne, S., Bürgi, C., & Davin, E. L. (2021). The role of urban trees in reducing land surface temperatures in European cities. *Nature Communications*, *12*(1), Article 1. https://doi.org/10.1038/s41467-021-26768-w

Schwingshackl, C., Hirschi, M., & Seneviratne, S. I. (2018). A theoretical approach to assess soil moisture–climate coupling across CMIP5 and GLACE-CMIP5 experiments. *Earth System Dynamics*, *9*(4), 1217–1234. https://doi.org/10.5194/esd-9-1217-2018

Seferian, R. (2018). *CNRM-CERFACS CNRM-ESM2-1 model output prepared for CMIP6 CMIP historical* [Data set]. Earth System Grid Federation. https://doi.org/10.22033/ESGF/CMIP6.4068

Séférian, R., Nabat, P., Michou, M., Saint-Martin, D., Voldoire, A., Colin, J., Decharme, B., Delire, C., Berthet, S., Chevallier, M., Sénési, S., Franchisteguy, L., Vial, J., Mallet, M., Joetzjer, E., Geoffroy, O., Guérémy, J.-F., Moine, M.-P., Msadek, R., … Madec, G. (2019). Evaluation of CNRM Earth System Model, CNRM-ESM2-1: Role of Earth System Processes in Present-Day and Future Climate. *Journal of Advances in Modeling Earth Systems*, *11*(12), 4182–4227. https://doi.org/10.1029/2019MS001791

Sellar, A. A., Jones, C. G., Mulcahy, J. P., Tang, Y., Yool, A., Wiltshire, A., O'Connor, F. M., Stringer, M., Hill, R., Palmieri, J., Woodward, S., de Mora, L., Kuhlbrodt, T., Rumbold, S. T., Kelley, D. I., Ellis, R., Johnson, C. E., Walton, J., Abraham, N. L., … Zerroukat, M. (2019). UKESM1: Description and Evaluation of the U.K. Earth System Model. *Journal of Advances in Modeling Earth Systems*, *11*(12), 4513–4558. https://doi.org/10.1029/2019MS001739

Sen, P. K. (1968). Estimates of the Regression Coefficient Based on Kendall's Tau. *Journal of the American Statistical Association*, *63*(324), 1379–1389. https://doi.org/10.1080/01621459.1968.10480934

Seneviratne, S. I., Corti, T., Davin, E. L., Hirschi, M., Jaeger, E. B., Lehner, I., Orlowsky, B., & Teuling, A. J. (2010). Investigating soil moisture–climate interactions in a changing climate: A review. *Earth-Science Reviews*, *99*(3), 125–161. https://doi.org/10.1016/j.earscirev.2010.02.004

Seneviratne, S. I., Donat, M. G., Mueller, B., & Alexander, L. V. (2014). No pause in the increase of hot temperature extremes. *Nature Climate Change*, *4*(3), Article 3. https://doi.org/10.1038/nclimate2145

https://doi.org/10.5194/egusphere-2023-1925
Preprint. Discussion started: 1 September 2023

Seneviratne, S. I., Lüthi, D., Litschi, M., & Schär, C. (2006). Land–atmosphere coupling and climate change in Europe. *Nature*, *443*(7108), Article 7108. https://doi.org/10.1038/nature05095

Seneviratne, S. I., Zhang, X., Adnan, M., Badi, W., Dereczynski, C., Di Luco, A., Ghosh, S., Iskandar, I., Kossin, J., Lewis, S., Otto, F., Pinto, I., Satoh, M., Vicente-Serrano, S. M., Wehner, M., & Zhou, B. (2021). *Climate Change 2021: The Physical Science Basis. Contribution of Working Group I to the Sixth Assessment Report of the Intergovernmental Panel on Climate Change* [[Masson-Delmotte, V., P. Zhai, A. Pirani, S.L. Connors, C. Péan, S. Berger, N. Caud, Y. Chen, L. Goldfarb, M.I. Gomis, M. Huang, K. Leitzell, E. Lonnoy, J.B.R. Matthews, T.K. Maycock, T. Waterfield, O. Yelekçi, R. Yu, and B. Zhou (eds.)]. Cambridge University Press. In Press.].

Sillmann, J., Thorarinsdottir, T., Keenlyside, N., Schaller, N., Alexander, L. V., Hegerl, G., Seneviratne, S. I., Vautard, R., Zhang, X., & Zwiers, F. W. (2017). Understanding, modeling and predicting weather and climate extremes: Challenges and opportunities. *Weather and Climate Extremes*, *18*, 65–74. https://doi.org/10.1016/j.wace.2017.10.003

Sippel, S., Zscheischler, J., Mahecha, M. D., Orth, R., Reichstein, M., Vogel, M., & Seneviratne, S. I. (2017). Refining multi-model projections of temperature extremes by evaluation against land–atmosphere coupling diagnostics. *Earth System Dynamics*, *8*(2), 387–403. https://doi.org/10.5194/esd-8-387-2017

Stegehuis, A. I., Vogel, M. M., Vautard, R., Ciais, P., Teuling, A. J., & Seneviratne, S. I. (2021). Early Summer Soil Moisture Contribution to Western European Summer Warming. *Journal of Geophysical Research: Atmospheres*, *126*(17), e2021JD034646. https://doi.org/10.1029/2021JD034646

Swart, N. C., Cole, J. N. S., Kharin, V. V., Lazare, M., Scinocca, J. F., Gillett, N. P., Anstey, J., Arora, V., Christian, J. R., Hanna, S., Jiao, Y., Lee, W. G., Majaess, F., Saenko, O. A., Seiler, C., Seinen, C., Shao, A., Sigmond, M., Solheim, L., … Winter, B. (2019). The Canadian Earth System Model version 5 (CanESM5.0.3). *Geoscientific Model Development*, *12*(11), 4823–4873. https://doi.org/10.5194/gmd-12-4823-2019

Swart, N. C., Cole, J. N. S., Kharin, V. V., Lazare, M., Scinocca, J. F., Gillett, N. P., Anstey, J., Arora, V., Christian, J. R., Jiao, Y., Lee, W. G., Majaess, F., Saenko, O. A., Seiler, C., Seinen, C., Shao, A., Solheim, L., von Salzen, K., Yang, D., … Sigmond, M. (2019a). *CCCma CanESM5 model output prepared for CMIP6 CMIP historical* [Data set]. Earth System Grid Federation. https://doi.org/10.22033/ESGF/CMIP6.3610

Swart, N. C., Cole, J. N. S., Kharin, V. V., Lazare, M., Scinocca, J. F., Gillett, N. P., Anstey, J., Arora, V., Christian, J. R., Jiao, Y., Lee, W. G., Majaess, F., Saenko, O. A., Seiler, C., Seinen, C., Shao, A., Solheim, L., von Salzen, K., Yang, D., … Sigmond, M. (2019b).

https://doi.org/10.5194/egusphere-2023-1925
Preprint. Discussion started: 1 September 2023

CCCma CanESM5 model output prepared for CMIP6 ScenarioMIP [Data set]. Earth System Grid Federation. https://doi.org/10.22033/ESGF/CMIP6.1317

Tachiiri, K., Abe, M., Hajima, T., Arakawa, O., Suzuki, T., Komuro, Y., Ogochi, K., Watanabe, M., Yamamoto, A., Tatebe, H., Noguchi, M. A., Ohgaito, R., Ito, A., Yamazaki, D., Ito, A., Takata, K., Watanabe, S., & Kawamiya, M. (2019). *MIROC MIROC-ES2L model output prepared for CMIP6 ScenarioMIP* [Data set]. Earth System Grid Federation. https://doi.org/10.22033/ESGF/CMIP6.936

Tang, Y., Rumbold, S., Ellis, R., Kelley, D., Mulcahy, J., Sellar, A., Walton, J., & Jones, C. (2019). *MOHC UKESM1.0-LL model output prepared for CMIP6 CMIP historical* [Data set]. Earth System Grid Federation. https://doi.org/10.22033/ESGF/CMIP6.6113

Teuling, A. J. (2018). A hot future for European droughts. *Nature Climate Change*, *8*(5), Article 5. https://doi.org/10.1038/s41558-018-0154-5

Teuling, A. J., Seneviratne, S. I., Stöckli, R., Reichstein, M., Moors, E., Ciais, P., Luyssaert, S., van den Hurk, B., Ammann, C., Bernhofer, C., Dellwik, E., Gianelle, D., Gielen, B., Grünwald, T., Klumpp, K., Montagnani, L., Moureaux, C., Sottocornola, M., & Wohlfahrt, G. (2010). Contrasting response of European forest and grassland energy exchange to heatwaves. *Nature Geoscience*, *3*(10), Article 10. https://doi.org/10.1038/ngeo950

Theil, H. (1992). A Rank-Invariant Method of Linear and Polynomial Regression Analysis. In B. Raj & J. Koerts (Eds.), *Henri Theil's Contributions to Economics and Econometrics: Econometric Theory and Methodology* (pp. 345–381). Springer Netherlands. https://doi.org/10.1007/978-94-011-2546-8_20

Thorarinsdottir, T. L., Sillmann, J., Haugen, M., Gissibl, N., & Sandstad, M. (2020). Evaluation of CMIP5 and CMIP6 simulations of historical surface air temperature extremes using proper evaluation methods. *Environmental Research Letters*, *15*(12), 124041. https://doi.org/10.1088/1748-9326/abc778

Trenberth, K. E., Fasullo, J. T., & Shepherd, T. G. (2015). Attribution of climate extreme events. *Nature Climate Change*, *5*(8), Article 8. https://doi.org/10.1038/nclimate2657

Ukkola, A. M., Kauwe, M. G. D., Pitman, A. J., Best, M. J., Abramowitz, G., Haverd, V., Decker, M., & Haughton, N. (2016). Land surface models systematically overestimate the intensity, duration and magnitude of seasonal-scale evaporative droughts. *Environmental Research Letters*, *11*(10), 104012. https://doi.org/10.1088/1748-9326/11/10/104012

Ukkola, A. M., Pitman, A. J., Donat, M. G., De Kauwe, M. G., & Angélil, O. (2018). Evaluating the Contribution of Land-Atmosphere Coupling to Heat Extremes in CMIP5 Models. *Geophysical Research Letters*, *45*(17), 9003–9012. https://doi.org/10.1029/2018GL079102

https://doi.org/10.5194/egusphere-2023-1925
Preprint. Discussion started: 1 September 2023

Ukkola, A. M., Prentice, I. C., Keenan, T. F., van Dijk, A. I. J. M., Viney, N. R., Myneni, R. B., & Bi, J. (2016). Reduced streamflow in water-stressed climates consistent with CO2 effects on vegetation. *Nature Climate Change*, *6*(1), Article 1. https://doi.org/10.1038/nclimate2831

Vogel, M. M., Hauser, M., & Seneviratne, S. I. (2020). Projected changes in hot, dry and wet extreme events' clusters in CMIP6 multi-model ensemble. *Environmental Research Letters*, *15*(9), 094021. https://doi.org/10.1088/1748-9326/ab90a7

Vogel, M. M., Orth, R., Cheruy, F., Hagemann, S., Lorenz, R., van den Hurk, B. J. J. M., & Seneviratne, S. I. (2017). Regional amplification of projected changes in extreme temperatures strongly controlled by soil moisture-temperature feedbacks. *Geophysical Research Letters*, *44*(3), 1511–1519. https://doi.org/10.1002/2016GL071235

Vogel, M. M., Zscheischler, J., & Seneviratne, S. I. (2018). Varying soil moisture–atmosphere feedbacks explain divergent temperature extremes and precipitation projections in central Europe. *Earth System Dynamics*, *9*(3), 1107–1125. https://doi.org/10.5194/esd-9-1107-2018

Vogel, M. M., Zscheischler, J., Wartenburger, R., Dee, D., & Seneviratne, S. I. (2019). Concurrent 2018 Hot Extremes Across Northern Hemisphere Due to Human-Induced Climate Change. *Earth's Future*, *7*(7), 692–703. https://doi.org/10.1029/2019EF001189

Voldoire, A. (2019). *CNRM-CERFACS CNRM-ESM2-1 model output prepared for CMIP6 ScenarioMIP ssp585* [Data set]. Earth System Grid Federation. https://doi.org/10.22033/ESGF/CMIP6.4226

Volodin, E. M., Mortikov, E. V., Kostrykin, S. V., Galin, V. Y., Lykossov, V. N., Gritsun, A. S., Diansky, N. A., Gusev, A. V., Iakovlev, N. G., Shestakova, A. A., & Emelina, S. V. (2018). Simulation of the modern climate using the INM-CM48 climate model. *Russian Journal of Numerical Analysis and Mathematical Modelling*, *33*(6), 367–374. https://doi.org/10.1515/rnam-2018-0032

Volodin, E., Mortikov, E., Gritsun, A., Lykossov, V., Galin, V., Diansky, N., Gusev, A., Kostrykin, S., Iakovlev, N., Shestakova, A., & Emelina, S. (2019a). *INM INM-CM4-8 model output prepared for CMIP6 CMIP historical* [Data set]. Earth System Grid Federation. https://doi.org/10.22033/ESGF/CMIP6.5069

Volodin, E., Mortikov, E., Gritsun, A., Lykossov, V., Galin, V., Diansky, N., Gusev, A., Kostrykin, S., Iakovlev, N., Shestakova, A., & Emelina, S. (2019b). *INM INM-CM4-8 model output prepared for CMIP6 ScenarioMIP* [Data set]. Earth System Grid Federation. https://doi.org/10.22033/ESGF/CMIP6.12321

Walker, A. P., De Kauwe, M. G., Bastos, A., Belmecheri, S., Georgiou, K., Keeling, R. F., McMahon, S. M., Medlyn, B. E., Moore, D. J. P., Norby, R. J., Zaehle, S., Anderson-Teixeira, K. J., Battipaglia, G., Brienen, R. J. W., Cabugao, K. G., Cailleret, M., Campbell, E., Canadell, J. G., Ciais, P., … Zuidema, P. A. (2021). Integrating the evidence for a terrestrial carbon sink caused by increasing atmospheric CO2. *New Phytologist*, *229*(5), 2413–2445. https://doi.org/10.1111/nph.16866

https://doi.org/10.5194/egusphere-2023-1925
Preprint. Discussion started: 1 September 2023

Wouters, H., Keune, J., Petrova, I. Y., van Heerwaarden, C. C., Teuling, A. J., Pal, J. S., Vilà-Guerau de Arellano, J., & Miralles, D. G. (2022). Soil drought can mitigate deadly heat stress thanks to a reduction of air humidity. *Science Advances*, *8*(1), eabe6653. https://doi.org/10.1126/sciadv.abe6653

Wu, T., Chu, M., Dong, M., Fang, Y., Jie, W., Li, J., Li, W., Liu, Q., Shi, X., Xin, X., Yan, J., Zhang, F., Zhang, J., Zhang, L., & Zhang, Y. (2018). *BCC BCC-CSM2MR model output prepared for CMIP6 CMIP historical* [Data set]. Earth System Grid Federation. https://doi.org/10.22033/ESGF/CMIP6.2948

Wu, T., Lu, Y., Fang, Y., Xin, X., Li, L., Li, W., Jie, W., Zhang, J., Liu, Y., Zhang, L., Zhang, F., Zhang, Y., Wu, F., Li, J., Chu, M., Wang, Z., Shi, X., Liu, X., Wei, M., … Liu, X. (2019). The Beijing Climate Center Climate System Model (BCC-CSM): The main progress from CMIP5 to CMIP6. *Geoscientific Model Development*, *12*(4), 1573–1600. https://doi.org/10.5194/gmd-12-1573-2019

Xin, X., Wu, T., Shi, X., Zhang, F., Li, J., Chu, M., Liu, Q., Yan, J., Ma, Q., & Wei, M. (2019). *BCC BCC-CSM2MR model output prepared for CMIP6 ScenarioMIP ssp370* [Data set]. Earth System Grid Federation. https://doi.org/10.22033/ESGF/CMIP6.3035

Zhu, Z., Piao, S., Myneni, R. B., Huang, M., Zeng, Z., Canadell, J. G., Ciais, P., Sitch, S., Friedlingstein, P., Arneth, A., Cao, C., Cheng, L., Kato, E., Koven, C., Li, Y., Lian, X., Liu, Y., Liu, R., Mao, J., … Zeng, N. (2016). Greening of the Earth and its drivers. *Nature Climate Change*, *6*(8), Article 8. https://doi.org/10.1038/nclimate3004